Energy Conversion and Management: X 30 (2026) 101785

Contents lists available at ScienceDirect

Energy Conversion and Management: X

journal homepage: www.sciencedirect.com/journal/energy-conversion-and-management-x

Hybrid energy storage through the passive connection of a Vanadium Redox Flow Battery and a supercapacitor: An experimental, modelling, economic and environmental impact assessment study

Monica Giovannucci [a], Elisabetta Petri [a], Alessandro Brilloni [a], Eva-Maria Heigl [b], Andreas Zauner [b], Estanis Oyarbide [c,d], Jiří Charvát [e], Francesca Soavi [a,f,*]

[a] Department of Chemistry "Giacomo Ciamician", Alma Mater Studiorum University of Bologna, via P. Gobetti 85, 40129 Bologna, Italy
[b] Energieinstitut an der Johannes Kepler Universität Linz, Altenberger Straße 69, 4040 Linz, Austria
[c] Epic Power Converters S.L., Grupo Gregorio Quejido, Calle F Oeste, Nave 93 Polígono Industrial Malpica, 50016 Zaragoza, Spain
[d] Aragon Institute of Engineering Research, University of Zaragoza, C/Mariano Esquillor s/n, 50018 Zaragoza, Spain
[e] New Technologies – Research Centre, University of West Bohemia, Univerzitní 8, 306 14 Plzeň, Czech Republic
[f] Center for the Environment, Energy, and Sea - Interdepartmental Centre for Industrial Research in Renewable Resources, Environment, Sea and Energy (CIRI-FRAME), Alma Mater Studiorum University of Bologna Viale Ciro Menotti, 48 - 48122 Marina di Ravenna (RA), Italy

ARTICLE INFO

Keywords:
Hybrid Energy Storage
Vanadium Redox Flow Battery
Supercapacitor
Modelling
Life Cycle & Economic Assessment
Passive Parallel Connection

ABSTRACT

Developing a Hybrid Energy Storage System (HESS) involves integrating technologies with complementary attributes. Coupling Redox Flow Batteries (RFBs) with Supercapacitors (SCs) emerges as one of the most promising options. For the first time at our knowledge, here we report about a study on the passive HESS VRFB-SC configuration that was investigated through experimental tests, modelling, life cycle and economic assessments. Indeed, we present a laboratory-sized HESS comprising a Vanadium Redox Flow Cell (VRFC) and a SC, directly connected in parallel without any power converter. Initially, individual tests were conducted on the standalone VRFB and SC using short discharge protocols (5 s). Subsequently, the two systems were interconnected in parallel and subjected to the same discharge protocol. An equivalent electrical model, resembling a parallel R-C circuit, was developed to elucidate the discharge mechanism of the direct parallel system. The tests revealed that the SC mitigates the VRFB's ohmic drop due to the transient behaviour of the R-C circuit. Furthermore, the hybrid system demonstrated enhanced energy delivery at higher currents compared to the standalone VRFB, a phenomenon elucidated by our proposed model. Additionally, the model facilitates the sizing of the SC relative to VRFB performance. In addition to technical findings, this article provides a comprehensive economic analysis and life cycle assessment (LCA) of the proposed system. These assessments highlight the potential cost-effectiveness and reduced global warming potential of the passively connected VRFB-SC HESS, underscoring its viability as a sustainable energy storage solution.

1. Introduction

Redox-flow batteries (RFBs) are among the most interesting technologies in the energy storage scenario. The design flexibility and the possibility to separately scale power and energy make them extremely attractive for the energy stakeholders [1].

Glossary: CAPEX, Capital Expenditure; EDLC, Electrochemical Double-Layer Capacitor; EMS, Energy Management System; ESR, Equivalent Series Resistance; FEP, Freshwater Eutrophication Potential; FETP, Freshwater Ecotoxicity Potential; GCPL, Galvanostatic Charge-Discharge with Potential Limitation; GWP, Global Warming Potential; HESS, Hybrid Energy Storage System; HTPc, Human Toxicity Potential, cancer effects; HTPnc, Human Toxicity Potential, non-cancer effects; LCI, Life Cycle Inventory; LCIA, Life Cycle Impact Assessment; LCA, Life Cycle Assessment; LCOS, Levelized Cost of Storage; LOP, Agricultural Land Occupation Potential; METP, Marine Ecotoxicity Potential; OCV, Open Circuit Voltage; PCS, Power Control System; PED, Primary Energy Demand; RFB, Redox Flow Battery; SC, Supercapacitor; SI, Supplementary Information; SOC, State of Charge; TETP, Terrestrial Ecotoxicity Potential; VRFB, Vanadium Redox Flow Battery; VRFC, Vanadium Redox Flow Cell; WiSE, Water in Salt Electrolyte; WCP, Water Consumption Potential.

* Corresponding author at: Department of Chemistry "Giacomo Ciamician", Alma Mater Studiorum University of Bologna, via P. Gobetti 85, 40129 Bologna, Italy.
E-mail address: francesca.soavi@unibo.it (F. Soavi).

https://doi.org/10.1016/j.ecmx.2026.101785
Received 11 March 2026; Accepted 17 March 2026
Available online 23 March 2026

RFBs have been proposed with different chemistries [2,3]. Among them, Vanadium Redox Flow Batteries (VRFBs) are the most widespread and marketed. VRFBs feature an energy density of 25–35 Wh L^{-1} and a long cycle life of 15 000–20 000 charge/discharge cycles. Power performance,that can be controlled by regulating the electrolyte flow, still need improvements being in the order of 100 mW cm^{-2} of electrode. Increasing energy and power performance of VRFBs is extremely important, because it will decrease the Levelized Costs of Storage (LCOS) of this technology that today is indicated in 0.18 € kWh^{-1} $cycle^{-1}$, 3 times higher than the 2023 European Commission target of 0.05 € kWh^{-1} $cycle^{-1}$ (10 000 cycles) [4,5].

An emerging approach to enhance performance, efficiency, and lifespan is by integrating VRFBs with diverse energy storage technologies within the so-called Hybrid Energy Storage Systems (HESSs). Shubert et al. conducted a comprehensive review of the different technologies currently available on the market, including Supercapacitors (SCs) and RFBs. They concluded that combining RFBs with SCs represents the most appropriate solution for HESS in terms of cycle and calendar lifetime, design flexibility, ecological impact, and safety. In addition, when comparing hybrid configurations in terms of self-discharge, systems combining RFB and SC demonstrates clear advantages due to low RFB daily self-discharge rate of 0.13% and high durability, with average cycle lives of 10^6 cycles for SC and 10^5 cycles for RFB. This combination also supports the widest range of storage durations, from milliseconds to several weeks. This makes it particularly suitable for complex applications, where energy systems must manage both rapid power fluctuations and longer-term energy balancing across multiple temporal scales [6]. An example is the HESS developed in the HyFlow project [7], that combined VRFB and supercapacitor technologies. This system ensures rapid and adaptable electricity availability by addressing peak demands from both private and public loads, as well as renewable energy production. Specifically, the HyFlow project aimed to design a storage solution suitable for applications ranging from microgrid level (5 kW) to industrial scale (300 kW) [7]. SCs are, indeed, distinguished by their high specific power (500–30 000 W kg^{-1}) and outstanding cycle-life (up to millions of cycles) [8,9]. The most commercialized SC technology, i.e. the electrochemical double-layer capacitors (EDLCs), store energy by a very fast and reversible electrostatic charge separation at the electrode surface/electrolyte interphase, without involving faradic reactions. However, the specific energy of SCs is one order of magnitude lower than that of batteries (2–8 Wh kg^{-1}) [8,9]. Hence, SCs are considered an expensive technology in terms of energy storage capability (>4500 € kWh^{-1}), but inexpensive in terms of power capability (<1 € kW^{-1}) [8]. Commercial SCs commonly employ expensive organic electrolyte solutions containing alkylammonium salts (e.g. tetraethylammonium tetrafluoroborate) in organic solvents (e.g. acetonitrile or propylene carbonate) that enable to achieve $V_{SC,max}$ up to 3 V but that contribute up to 27% of the overall SC cost [8]. Hence, alternative electrolytes are being investigated to meet performance and safety requirements. Aqueous electrolytes appear promising due to their non-flammability, cost-effectiveness, and environmental friendliness. However, water electrolysis in conventional aqueous solutions (acidic, alkaline or neutral) limits $V_{SC,max}$ below 2 V [10]. An interesting option is represented by water-in-salt electrolytes (WiSE) that offer a wide electrochemical stability window and high conductivity [11]. Notably, a solution with a concentration of 30 mol kg^{-1} of ammonium acetate can yield an electrochemical stability window of 3.2 V and a conductivity of 25 mS cm^{-1} [12].

The most common scheme of linking batteries and supercapacitors typically employs a bidirectional power converter [6]. This converter facilitates bidirectional power flow management within the system [13]. However, in literature, few studies report about the direct connection between batteries and supercapacitors. This type of connection is termed “passive” [14,15] and consists in the parallel connection between different storage systems that does not employ a power converter. While an active topology, such as that of the HyFlow project, can be used in microgrids and industrial applications, according to the literature a passive topology can be implemented in diverse applications, including pulsed current [16] and vehicle applications [17].

In Ref. [14], it is shown that the power converter-based (or “active”) connection offers several advantages over the passive one, such as battery current peaks reduction and DC bus voltage control. In Ref. [18] it is shown that the autonomy of a device powered by a HESS based on a battery and a parallel connected supercapacitor bank, is improved because the supercapacitor decreases the HESS internal resistance. Furthermore, the connection of the battery to the supercapacitor by a DC-DC converter enables the use of lower voltage supercapacitor banks, hence a lower number of SC cells. Therefore, the use of a DC-DC converter appears to be a cost-effective option, since it allows the use of reduced number of EDLC cells while maintaining a comparable performance. However, power converters decrease HESS efficiency and hence might impact on power cost. Indeed, the power converters might cause 50% of power losses [14]. Ref. [19] compares efficiencies of 26 types of DC/DC converters and shows that most of them exhibit efficiencies between 92% and 98.5%.

The studies discussed above were carried out by considering “closed” battery (e.g. lithium-ion batteries) and supercapacitor packs, as separate elements, each one of them made of different stacks embedded in different cases. To date, there are no studies focusing on the passive connection of emerging technologies such as RFBs and SCs, as well as detailed LCA (life cycle assessment) and economic analyses of HESSs based on these storage units are not available.

Hence the aim of this study is to investigate and model the electrical behaviour of a HESS based on the passive, parallel connection of a Vanadium Redox Flow cell (VRFC) and an SC cell, while providing an assessment of the economics and environmental impacts of a hypothetical upscaled system. We report about the electrochemical tests carried out on the single VRFC and SC cells units and of the VFRC-SC HESS. We tested the integration of the VRFC and SCs at cell level and laboratory scale. The standalone VRFC and SCs served as control groups. Such monolithically integrated system has been evaluated by short-galvanostatic discharges to assess energy and capacitance performance. The pulsed test validates the system for applications characterised by power peaks on a timescale of seconds, such as the load profile of an electric city bus. In addition, we propose a simple methodology and a semi-empirical model that enables to design the VRFC-SC HESS by taking into account relevant VRFC and SC cell parameters (e.g. sizes, current rate, ESR, capacitance). The literature offers various methodologies for modelling VRFC and SC [20,21], but an equivalent circuit that models the passive connected VRFC-SC system is not available yet. Here, we propose a simple equivalent model, while being aware of the potential increased error compared to more complex models. Our aim is, indeed, to propose a simple tool that allows sizing the hybrid VRFC-SC system based on common parameters that can be easily derived from the VRFC and SC datasheets.

In addition to experimental characterization and modelling, this work incorporates the assessment of economic and environmental impacts of the proposed HESS with passive connection compared to a HESS with converter-based connection. These evaluations aim to provide a comprehensive understanding of the system's feasibility and sustainability, which is required by the European Battery Regulation [22]. The economic assessment considers key cost drivers, such as the components’ capital expenses and operational requirements, whereas the LCA conducted in this study focuses on quantifying environmental impacts of the system’s production and use phase. Overall, the aim of our experimental and modelling work is to demonstrate that the parallel passive connection at cell level of the VRFC with a SC: i) is a simple approach that enables to boost energy and current rate response under short discharge pulses, ii) does not require high-voltage SCs, such as the commercial ones that feature organic electrolytes, iii) needs an equivalent electric model as a tool to forecast the behaviour of the system varying the SC size, and iv) is superior to a comparable system with

converter-based connection regarding costs and environmental impacts (specifically for GWP).

We would like to clarify that the objective of this study is not to provide a complete design of a HESS based on VRFB and SC. Instead, we present an exploratory investigation aimed at assessing the potential to combine these two technologies in a passive configuration. This preliminary analysis intends to offer insights that may support future research and development in this area.

2. Materials and methods

2.1. VRFC and SC cells

This section reports the specifications of the devices under examination, along with their corresponding characterization. The devices involved in the study comprise a VRFC (discussed in Section 2.1.1), and different commercially available SCs (outlined in Section 2.1.2). Section 2.1.3 describes the test protocols and Section 2.1.4 elaborates the proposed equivalent electric model.

2.1.1. Vanadium redox flow cell nominal characteristics and assembly

The company Pinflow provided the cell used during the test. This cell possesses an exchange (electrode) surface area of 4 cm^2, operates within a voltage range of 1.65 V to 0.8 V, and supports a maximum discharging current of 2 A. A total of 100 mL electrolyte (50 mL for the anolyte and 50 mL for the catholyte) was contained in two tanks. The theoretical calculated capacity of the cell is 2144 mAh. Further specifications are detailed in Table 1.

The assembly of the cell is shown in the exploded view drawing in Fig. S1. Table S1 reports the coulombic, energy and voltage efficiency of the cell varying the current density. The structure of both sides of the cell comprises layers arranged as follows: an end plate with an insulating plane, a copper current collector, a carbon-polymer composite plate, a seal, the flow frame with fittings, a membrane seal, and a felt electrode; in the middle between the two sides there is the membrane positioned centrally. After the assembly, the cell was operated with the electrolyte which consisted of 1.6 mol dm^{-3} of vanadium (equimolar mixture of vanadium in oxidation states III and IV), 2 mol dm^{-3} of H_2SO_4 and 0.3% of H_3PO_4. Two peristaltic pumps, Watson–Marlow 120S/DV, operate at 40 to 60 rpm, ensuring a catholyte and anolyte flow rates within the interval 40–60 mL min^{-1}. This flow rate was set in order to facilitate mass transport, especially at the highest current. Argon was used to purge the cell for 30 min before electrochemical tests.

Initially, the vanadium electrolyte is equal for both the positive and negative electrodes, featuring an indicative state of charge of a −50%. To activate the electrolyte, the cell went through an activation process. Initially, the cell was charged at 400 mA up to its theoretical capacity (2 144 mAh). Subsequently, the cell underwent cycles of charge and discharge, and when it achieved a coulombic efficiency of at least 95%, the cell was considered prepared to proceed to subsequent testing phases that are described in Section 2.1.3.

2.1.2. Commercial supercapacitors nominal characteristics

Various commercial supercapacitors, purchased from EATON, based on high surface area carbons and organic electrolyte, were considered in this study. We employed commercial supercapacitors because of their availability and reliability. The selection of the SCs was based on ensuring that their operating currents were of the same order of magnitude as the operating currents of the VRFC. The capacitance C, the equivalent series resistance (ESR), the maximum cell voltage ($V_{SC,max}$) and maximum continuous discharge current, and leakage currents derived from the datasheet of the manufacturer, are outlined in Table 2 along with the maximum energy ($W_{SC,max}$) and the maximum power ($P_{SC,max}$) that were calculated according to the Eqs. (1) and (2).

$$W_{SC,max} = \frac{1}{2} C V_{SC,max}^2 \tag{1}$$

$$P_{SC,max} = \frac{1}{4} \frac{V_{SC,max}^2}{ESR_{SC}} \tag{2}$$

Notably, the primary distinction lies in the nominal capacitance, ranging from 1 F to 100 F. The 9 F SC was built through a parallel direct connection of three distinct supercapacitors: one rated at 1 F, another at 3 F, and a third at 5 F. The related characteristics were deduced from those of the individual supercapacitor units and subsequently confirmed through galvanostatic tests. All commercial supercapacitors can operate up to 2.7 V and exhibit ESRs that diminish with increasing capacitance, ranging from 0.2 Ω to 0.011 Ω as the capacitance moves from 1 F to 100 F.

Table 1
Nominal values of exchange surface, cell voltage range, theoretical capacity (50 mL tanks), and maximum discharging current of the Pinflow VRF Cell.

Surface	Cell voltage range	Theoretical Capacity	Maximum discharging current
cm^2	*V*	*mAh*	*A*
4	0.8–1.65	2 144	2

2.1.3. Pulse galvanostatic discharges

The electrochemical tests were carried out using a VSP multichannel potentiostat/galvanostat (Bio-Logic Science Instruments) under ambient conditions. Data were analysed by the Bio-Logic software EC-Lab 10.23. The charging phases was conducted with unplugged VRFC and SC. Only when the VRFC was charged, it was connected with the SC and the pulsed current protocol was applied. Both the individual VRFC and SC devices and the VRFC-SC underwent similar galvanostatic pulse tests to collect useful data for a comparison, as described below. The main test conducted on the different charged devices consisted in a pulsed galvanostatic discharge (GCPL) lasting 5 s, that was repeated at different current rates. For both the VRFC and the VRFC-SC, the current profile observes a stepwise pattern: for the initial 5 s, neither voltage nor current was applied, maintaining the system in Open Circuit Voltage (OCV) at ca. 1.5 V; starting from the fifth second, the cell was galvanostatically discharged with a discharge time cut-off of 5 s and a discharge voltage cut-off of 0.8 V; thereafter, the test was concluded (Fig. S2a in the Supplementary Information file). In the case of the standalone SC, an initial charging step was undertaken to attain the maximum voltage. Subsequently, the SC was maintained at this voltage for a duration of 10 s, during which it is evident (as depicted in Fig. S2b) that the current is not zero. Following this phase, the SC underwent a 5-second pulsed discharge, similarly to the testing procedure conducted on both the VRFC and the VRFC-SC system. Also in this case a voltage cut-off of 0.8 V was applied.

2.1.4. Equivalent electric model

Fig. 1a illustrates the simplified equivalent circuit adopted in this study to model the VRFC-SC parallel connected hybrid system. Given the inherent simplicity of this model, the analysis does not consider influencing factors such as temperature and polarisation effects. A constant voltage source (V_b) in series with a resistance R_b represents the equivalent circuit branch of the VRFC battery according to the Rint Model for batteries [23]. A capacitance (C) in series with the equivalent series resistance R_{SC} describes the SC [24]. The two blocks are connected in parallel, mirroring the VRFC-SC system. The VRFC-SC block is then connected to the external load that is configured to emulate the constant current discharge, denoted as i_L. The currents flowing in the SC and VRFC branches are named respectively i_{SC} and i_b. The voltage measured at the two ends of each branch assumes the same value, named as v_L.

The model attempts to achieve various purposes. Firstly, it aims to enhance understanding of the system by elucidating aspects such as how the current flows in the branches and the influence of the devices ESRs

Table 2
Commercial Supercapacitors characteristics purchased from Eaton. Data, except for maximum energy and power, are derived from the datasheets of the manufacturer.

Acronym	Capacitance	ESR	$V_{SC,max}$	$W_{SC,max}$	$P_{SC,max}$	Maximum continuous discharging current	Leakage currents
	F	Ω	*V*	*mWh*	*W*	*A*	*μA*
SC1F	1	0.200	2.7	1	9.1	0.8	10
SC3F	3	0.080	2.7	2	23	1.6	15
SC5F	5	0.040	2.7	5.1	46	2.3	20
SC9F[a]	9[a]	0.023[a]	2.7	8.8[a]	46[a]	2.3[a]	23
SC34F	34	0.016	3.0	42.5	141	6.5	75
SC100F	100	0.011	3.0	125	205	11.7	225

[a] Values for 9 F supercapacitor were calculated by experimental tests.

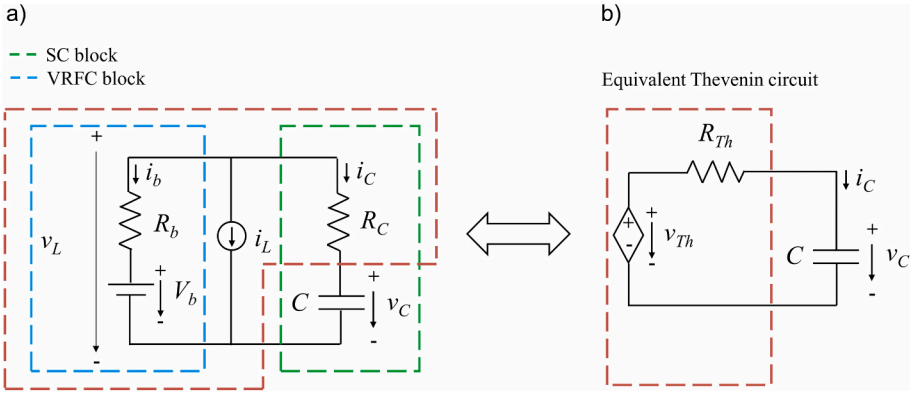

Fig. 1. a) equivalent electric circuit and b) equivalent thevenin circuit for the VRFC-SC HESS.

and SC capacitance on system behaviour. Secondly, the model should permit the determination of the time-dependent voltage profile during the discharging phase. Indeed, in an R-C circuit like this, it is essential to evaluate the time constant of the system. Finally, this simplified model aims to allow sizing the SC, in terms of capacitance to be combined with the VRFC for improved energy delivery during pulsed discharge. Addressing these objectives necessitates the development of a mathematical model describing the evolution of current and voltage over time. Indeed, due to the presence of capacitance within the system, both current and voltage values vary with time exhibiting transient behaviour. To derive an analytical solution for the circuit, the Thevenin theorem facilitates the transformation of the parallel circuit into the corresponding Thevenin circuit of Fig. 1b, comprising a single loop. Subsequently, Kirchhoff's laws are employed to formulate the Equations. Solving these Equations permits the determination of the system's time constant, while their solutions elucidate the temporal evolution of currents and voltages. The implementation of Thevenin Theorem and Kirchhoff's laws is described in the Supplemental Information file.

The Thevenin circuit is a simple R-C transient circuit with a well-known solution reported in Eq. (3) with a time constant given by $\tau = R_{th}C$.

$$i_{SC}(t) = I_{SC}(0)\exp(-t/\tau) \tag{3}$$

Eq. (3) gives the value over time of the current in the SC branch (i_{SC}); the current flows following an exponential behaviour from the initial value $I_{SC}(0) = [V_{Th}(0)\text{-}V_{SC}(0)]/R_{Th}$.

Once computed the SC current and using the original circuit of Fig. 1a it is straightforward to compute the VRFC current i_b (Eq. (4)) and the measurable load voltage v_L (Eq. (5)).

$$i_b(t) = -i_L(t) - i_{SC}(t) \tag{4}$$

$$v_L(t) = v_b + i_b(t)R_b \tag{5}$$

Managing all the Equations from Eq. (3) to (5) it is possible to describe currents and voltages of the whole equivalent circuit. The Equations obtained in this section have been implemented in the software Matlab to provide a numerical solution for the analysis depicted in the discussion section.

2.2. Life cycle assessment

This section reports on the life cycle assessment of a HESS, comparing a converter-based connection between VRFB and SC, to a passive connection. The LCA was conducted following the ISO 14040/14044 LCA standards [25,26]. In the goal and scope definition, the study's purpose was outlined (Section 2.2.1) and in the life cycle inventory (LCI) analysis data on process inputs and outputs (masses, energy) were collected (Section 2.2.2). Subsequently, LCI results were translated into environmental impacts in the life cycle impact assessment phase (LCIA), applying a harmonized LCIA methodology. LCIA results were then discussed and further investigated in a sensitivity analysis (Section 2.2.3). This was complemented by a discussion of the limitations of the study and an outlook regarding potential further research needs. The LCA process was iterative, ensuring its continuous improvement and alignment between the different phases. For a deeper understanding of LCA methodologies, please refer to the works of Frischknecht et al. (2020) [27], Guinee et al. (Ed.) (2002) [28], Curran (Ed.) (2014) [29] and Klöpffer and Grahl (2014) [30]. Data used for the LCA presented in this study were to a large extent developed in HyFlow and adapted to the new system specifications [31].

2.2.1. Goal, scope and functional unit

The goal of this LCA study was to compare the environmental impacts of the production and use phase of a HESS with a converter-based connection between a VRFB and a SC, to a HESS with a direct connection. In case of a direct connection, no bidirectional DC-DC converters are required, but a higher number of SC cells than for a converter-based connection are used. To obtain results of practical interest, we projected the SC and VRFB to a realistic MW-scale. In the base case, we investigated a HESS integrating a 1 MW/4 MWh VRFB with a 2.5 MW SC, with either a converter-based or a direct connection (Table 3). In case of the direct connection, it has been considered that SC cells are charged only

Table 3
HESS parameters for the base case and for the sensitivity analysis.

	VRFB			SC[a]			AC-DC[b]			DC-DC[c]	EMS[d]	Cabling[e]
Converter-based (A)	x			x			x			x	x	x
Passive (B)	x			x			x				x	x
Configuration	Power [MW]	Energy [MWh]	Mass [t]	Power [MW]	Mass a[1)] [t]	Mass b[1)] [t]	Power [MW]	Mass [t]	Power [MW]	Mass [t]	Mass [t]	Mass [t]
Base case	1	4	299	2.5	2.2	6.5	3.5	21	1 + 2.5	5.5	0.4	0.3
Sensitivity 1				5	4.3	12.9	6	36	1 + 5	9.4	0.4	0.4
Sensitivity 2				10	6.5	19.4	11	66	1 + 10	17	0.4	0.5
Sensitivity 3				20	8.6	25.9	21	126	1 + 20	33	0.8	0.6
Sensitivity 4				40	10.8	32.4	41	246	1 + 40	64	1.5	0.7
Sensitivity 5				80	12.9	38.8	81	486	1 + 80	127	3	0.8

[a] Mass a = SC for converter-based connection, mass b = SC for passive connection (3x number of cells of SC for converter-based connection) − SC5F cell specifications, Table 2.
[b] AC-DC Inverter. LCI dataset: "GLO: market for inverter, 500 kW ecoinvent 3.8" [30] linearly upscaled by inversion power.
[c] DC-DC converters NOT included in HESS with direct connection between VRFB and SC.
[d] Approximated with LCI datasets for control cabinet (1 piece/10 MW SC assumed) and 1 computer: "GLO: market for control cabinet, heat and power co-generation unit, 160 kW electrical ecoinvent 3.8" AND "GLO: market for computer, desktop, without screen ecoinvent 3.8"[30].
[e] Estimated values.

up to 1.65 V of the maximum value of 2.7 V. Consequently, as for Eq. (2), the deliverable maximum power is approximately one third of the nominal power. Hence, to achieve the target power of the different HESS configurations listed in Table 3, the number of SC cells connected in parallel must triplicate.

In addition to the VRFB and SC, and the DC-DC converters in case of a converter-based connection, the HESS also employs an AC-DC inverter for connection to the energy source/sink, an energy management system (EMS) and power and data cabling. Foundations or housing were not accounted for in the LCA. The LCA of the production phase started from basic processes such as raw materials mining or energy generation, followed by parts production and final HESS assembly, including all transport steps. The use phase was modelled for a system lifetime of 20 years and 20 000 full cycles of charging/discharging, respectively. The production and use of the HESS were assumed to take place in Europe. The end-of-life phase of the HESS was not accounted for. The functional unit of this study was 1 kWh of energy discharged by the HESS over its lifetime.

2.2.2. Life cycle inventory

This LCA partly builds on data from a previous HyFlow publication [31], which were adapted to the new system specifications. The LCI of the SC, however, was not derived from HyFlow, as a different kind of SC was employed there. Instead, we used an activated carbon-acetonitrile SC, as published by Jiao et al. (2023) [32]. All underlying inventories are reported in the Supplementary Information (SI). Moreover, we expect that substituting the acetonitrile electrolyte by an aqueous electrolyte could further reduce the SC's environmental impacts. Therefore, we conducted an LCA comparing 1 kg of acetonitrile with 1 kg of WiSE ammonium acetate electrolyte (30 mol/kg) [12]. We assume that a 1:1 mass substitution of these two electrolyte types in the current SC design would be valid, a point that still requires experimental confirmation. The use phase of an energy storage system is shaped by the energy losses that occur during charging and discharging. These losses depend on the specific use case of the HESS and the individual energy efficiencies of its single components. In our preceding study [31], we showed that the theoretical roundtrip efficiency of the HESS with active connection can range from 43% to 79%, depending on the storage pathway. The same methodology was now applied to a HESS with passive connection, resulting in a theoretical round-trip efficiency between 64% and 89%. Potential losses specifically arising from the passive connection are not included here but are addressed in a sensitivity analysis. For this study, we considered a simplified use case in which all electricity is charged through the VRFB and then discharged through the SC. This results in a round-trip efficiency of 51% for an active connection and of 67% for a passive connection (Table S6, SI). Based on these considerations, the lifetime discharged energy, and the energy losses of the HESS, were determined as 54 040 MWh and 51 921 MWh in case of the active (converter-based) connection, and as 64 192 MWh and 31 617 MWh in case of the passive connection. For LCA modelling and LCI background datasets, the LCA for Experts 10.7 software and professional database by Sphera [33] and the ecoinvent 3.8 database [34] were used. European LCI background datasets were applied, if available. The use phase was modelled for a HESS cycle life of 20 000 full charging and discharging cycles over 20 years, following Blume et al. (2022) [35].

Moreover, the transport of the finalized HESS to a user in Europe and one exchange of the VRFB-stack [36], of the SC and of the AC-DC inverter after 10 years of operation, were accounted for [31]. The HESS was modelled to be charged with European photovoltaic power.

2.2.3. Life cycle impact assessment and sensitivity analysis

To translate the results of the LCI analysis into environmental impacts, we employed the acknowledged ReCiPe 2016 q(H) v1.1 methodology [37]. ReCiPe 2016 investigates environmental impacts in 18 midpoint categories, such as climate change, ozone depletion, and ecotoxicity. In this article, we focused on climate change with its indicator global warming potential (GWP). Moreover, the primary energy demand (PED) was assessed based on the cumulative energy approach [38,39]. A full list of investigated indicators, and all LCIA results, are provided in the SI. In a sensitivity analysis, we increased the SC size in five steps by 100%, 300%, 700%, 1 500% and 3 100% up to 80 MW, while leaving the VRFB specifications the same (Table 3). Thus, we assessed for both connection types, how a change of the system's power influenced its environmental impacts. Another sensitivity analysis was performed on the base configuration of the passively connected HESS, altering its roundtrip-efficiency from 67% to 62, 57 and 52%. In this way, we investigated how potential losses arising from the passive connection might impact the environmental performance of this type of HESS. The impact of varying the round-trip efficiency of the converter-based HESS was already examined through sensitivity analysis in our previous publication [31].

2.3. Economic assessment

Accurate forecasting of total project costs is pivotal for the planning and implementation of complex systems such as HESS. In contrast to simple cost aggregation approaches, total project costs cannot be derived solely from the costs of the main components (VRFB, SC, and

PCS), but must also include additional and indirect cost elements, such as engineering, civil works, component assembly, and commissioning, which significantly influence overall cost of the system. In industrial plant engineering, total project costs are commonly estimated using surcharge factor methods, such as the Total Factor Method (Lang Factor Method) or Single Factor Methods, which are based on empirical data and historical experience, cf. e.g., [40–43]. As HESS construction differs from conventional industrial plants, these methods, particularly the surcharge factors, cannot be directly transferred and therefore require adaptation. Accordingly, total project costs C_T were calculated as the sum of direct plant costs C_D and indirect plant costs C_I as expressed in the Equation C_T=$C_D + C_I$. Direct plant costs C_D=$C_M + C_A$ comprise the costs of the main components C_M (where C_C is the cost of one main component) and additional plant costs C_A, with the latter estimated by applying surcharge factors for direct costs f_d. Indirect plant costs C_I were derived by applying surcharge factors to the direct plant costs f_{id} (Eqs. (6) to (8)). The applied surcharge factors are summarized in Table S10.

$$C_M = \sum_{i=1}^{x} C_{Cx} \tag{6}$$

$$C_A = \sum_{i=1}^{x} (C_M{}^{*} f_{dx}) \tag{7}$$

$$C_I = \sum_{i=1}^{x} (C_D{}^{*} f_{idx}) \tag{8}$$

Due to the limited number of realized HESS installations of this kind, no dedicated historical data for surcharge factors are available. Therefore, the factors were estimated based on conventional industrial plant engineering and adjusted to reflect the higher degree of prefabrication of HESS components and their typically containerized delivery, which reduces assembly complexity and structural engineering requirements. Nevertheless, basic civil infrastructure remains necessary. To assess the influence of system size (power and storage capacity) and the power ratio between VRFB and SC, several HESS configurations were analysed. The VRFB size was kept constant, while the SC power was varied (see Section 2.2). Table 4 presents the CAPEX of the main components (for detail see [44]; the cost estimation for an SC with an aqueous electrolyte was based on the assumption that approximately 40% [8] of the total cost of an SC is attributed to the electrolyte. Given that the cost of an aqueous electrolyte is estimated to be only about one-tenth [12] of that of a conventional organic electrolyte, the total SC cost was adjusted accordingly) which were used to calculate the total project costs. As an illustrative example, the CAPEX for the reference HESS configuration (Base: SC 2.5 MW /VRFB 1 MW/4 MWh) is presented for the years 2022 and 2050, considering different connection types (active/passive) and SC types (organic/aqueous).

3. Results & discussion

3.1. VRFC-SC tests and modelling

This section reports about the results obtained performing the pulsed discharging test on the standalone VRFC (section 3.1.1), standalone SCs (section 3.1.2) and the parallel systems consisting of VRFC and the commercial SCs (section 3.1.3). Sections 3.1.4 and 3.1.5 report the modelling results showing also some insights. Section 3.1.6 compares test and modelling data.

3.1.1. VRFC test

The pulsed discharge was configured using the pulse galvanostatic discharge protocol reported in section 2.1.3 and depicted in Fig. S2a. The VRFC underwent testing across various currents ranging from 200 mA to 4 A, with increments of 100 mA. The discharge voltage cut-off was set at 0.8 V. Fig. 2a displays selected discharge voltage profiles of the VRFC at different current levels. The Figure emphasizes that the maximum practical current for the VRFC is 2 A. Indeed, at currents exceeding 2 A (i.e 4 A) the cell voltage drops below the cut-off threshold in less than 5 s of discharge. R_b was calculated at each current using the measured voltage drop (ΔV_b) values according to the Equation $R_b = \Delta V_b/i_L = (V_{OCV}\text{-}V)/i_L$ in which i_L is the value of the applied discharging current, V is the potential after the ohmic drop and V_{OCV} the OCV potential value of the cell. The energy delivered over the pulse discharge (W_{pulse}), was quantified at each current by the Eq. (9) (in Wh).

$$W_{pulse} = \frac{1}{3600} i_L \int_0^t v_L(t)dt \tag{9}$$

where v_L is the voltage. The discharging curves and the numerical results are respectively reported in Fig. 2a and Table S12. The VRFC delivered energy ranged from 0.4 mWh at 200 mA to 1.3 mWh at 2 A. The ohmic drop increased from 74 mV at 200 mA to 0.65 V at 2 A: this high value limits the discharge because the cut-off voltage (0.8 V) is reached more quickly. The R_b value settles in a range between 0.33 and 0.37 Ω.

3.1.2. Commercial SC test

As reported in section 2.1.3 and depicted in Fig. S2b, we subjected the supercapacitors to the following protocol: galvanostatic charging at 1.5 V (selected for comparability with the OCV exhibited by the tested VRFC), followed by a potential step to 1.5 V maintained for few seconds, and subsequent galvanostatic discharge with a cell cut-off voltage of 0.8 V and a cut-off discharge duration of 5 s. Discharge ceased upon reaching either of the specified cut-offs. Both charging and discharging steps were conducted at varying currents ranging from 400 mA to 10 A. As an example, Fig. 2b reports the galvanostatic discharge profiles of SC34F. The voltage decreases linearly over time, indicating that the discharge is driven solely by an electrical double layer process. These devices display behaviour similar to that of an ideal capacitor that is in series with a negligible ESR. As expected, the slope (dv_{SC}/dt) of the discharge profile over time increases with the current; this trend is explained by Eq. (10).

Table 4
CAPEX of the main components of the HESS "Base" configuration for the year 2022 and 2050 with different connection types active/passive and SC types organic/aqueous.

Year	Configuration	Connection	Component CAPEX [€]				
			SC	**DC-DC converterVRFB**	**DC-DC converterSC**	**AC-DCinverter**	**VRFB**
2022	**Base**	active/organic	127 935	121 500	210 543	253 975	1 676 524
		passive/organic	383 806	0	0		
		passive/aqueous	245 636	0	0		
2050	**Base**	active/organic	67 456	64 570	111 891	134 973	707 871
		passive/organic	202 367	0	0		
		passive/aqueous	129 515	0	0		

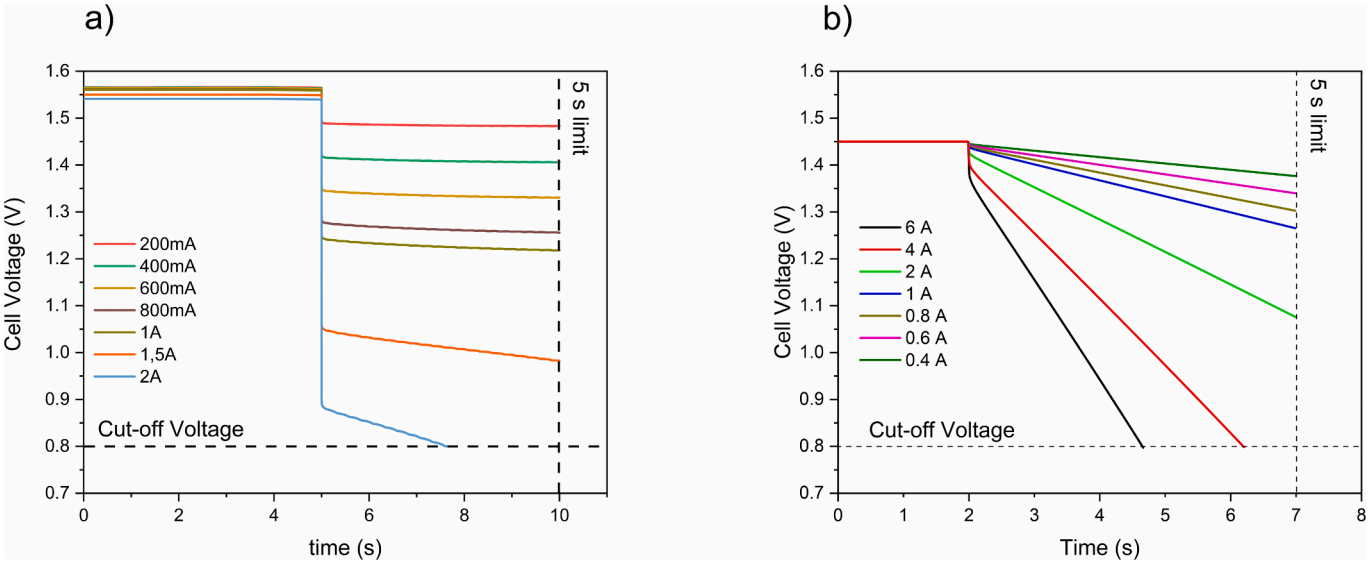

Fig. 2. a) voltage profile of VRFC during 5 s discharge at different currents at RT; b). Voltage profiles of SC34F under pulsed discharge curves of 5 s at different currents. Experimental tests were conducted at RT The starting SOC of the VRFC is 100%.

$$v_{SC} = \frac{Q}{C} \rightarrow \frac{dv_{SC}}{dt} = \frac{1}{C}\frac{dQ}{dt} = \frac{1}{C} i_{SC} \quad (10)$$

The ohmic drop ($\Delta v_{SC,Ohmic}$) at the beginning of discharge also increases with the current, following the Equation $\Delta v_{SC,Ohmic} = i_L R_{SC}$.

3.1.3. Hybrid VRFC-SC system test

Four distinct systems were evaluated. All featured the same VRFC, but different SCs of 5F, 9F, 34F, and 100F. The corresponding acronyms are: VRFC-SC5F, VRFC-SC9F, VRFC-SC34F, and VRFC-SC100F. As outlined in section 2.1.3, pulse tests protocol similar to that conducted on the VRFC (Fig. S2a), were performed on the VRFC-SC system, with the commercial SC connected in parallel with the vanadium cell. The parallel connection between the VRFC and the SC was established using a four-terminal configuration that was adopted to minimise the influence of external resistances. The initial phase involves charging the VRFC to full capacity at a rate of 600 mA, until reaching the designated cut-off charging voltage of 1.65 V, which is maintained for 5 min. Subsequently, the VRFC-SC system is left in open circuit, and the corresponding open circuit voltage of the system is recorded. Following this, a GCPL is executed at a defined current (i_L), with time and discharge voltage cut-offs set at 5 s and 0.8 V, respectively. The discharge profiles of the four tested systems are depicted in Fig. 3 (a, b, c, d). It is worth noting that the value of the capacitance highly impacts on the curve trend: the higher is the capacitance, the more linear is the profile. In addition, there is a high reduction of the Ohmic drop. These two effects (more linear profile and ohmic drop reduction) enable the possibility of discharging at higher currents. To deepen the effect of the capacitance on the system, Fig. 3e reports a comparison of the discharge curves at 2 A of the individual VRFC, the single SC34F and the hybrid VRFC-SC34F system.

When the two systems are directly connected in parallel, two phenomena become evident:

- a significant reduction in the ohmic drop compared to that observed with the standalone VRFC.
- the discharge profile exhibits a linear decrease over time, resembling that of the standalone SC but with a smaller slope than the SC (at the same current), suggesting an "apparent" increase in the overall system capacitance relative to the standalone SC. The entity of the reduction in the ohmic drop and the capacitive response depends respectively on the ESR and on the capacitance of the combined SC.

These behaviours can be elucidated by referring to the equivalent circuits reported in section 2.1.4 and that will be discussed in Section 3.1.4.

The discharge profiles were analysed to extract significant data such as delivered energy and power. Fig. 3f compares the amount of the energy delivered over 5-second galvanostatic pulses with the increase in currents for the VRFC and VRFC-SC systems featuring different SCs. The Figure clearly illustrates that the reduction in the ohmic drop and the apparent increase in capacitance enhance the energy performance of the hybrid system, which significantly outperforms the standalone VRFC at the highest currents. The energy gain is more pronounced when SCs with higher capacitance are connected. By incorporating the SC100 F, it is possible to conduct 5-second pulse discharges at 10 A, i.e., at a current regime five times greater than that achievable for the standalone VRFC, while delivering approximately 8–10 times more energy.

With regard to efficiency, we would like to emphasize that Table S1 presents the performance of the VRFC cell. Although we did not measure the charge–discharge cycle efficiency, it is important to note that the SC operates only during the initial phase of the discharge. Therefore, we assume that its impact on the overall efficiency is minimal. In addition, reducing the operating voltage of the SCs generates a non-accessible energy amount that can be evaluated through Eq. S1; specifically, decreasing the operating voltage from 2.7 to 1.5 V results in a non-accessible energy amount of approximately 70%. As an example, Fig. S5 reports examples of the discharge profiles of VRFC-SC systems during discharges longer than 5 s. It shows that after the first seconds the system voltage decreases until it reaches the VRFC voltage. This result indicates that the supercapacitor never fully discharges, as it cannot reach zero voltage because it is connected in parallel with the VRFC. Fig. S6 depicts the voltage profile during a continuous pulsed discharge of the VRFC-SC34F system. Each 800 mA pulse is followed by 1 min of rest (I = 0 mA), during which the system voltage returns to the value imposed by the VRFC open-circuit voltage (OCV). In addition, the SC benefit remains evident after several cycles, as the system consistently exhibits the absence of an ohmic drop over more than 30 000 s.

In addition, the leakage currents of the SCs investigated in this study are lower than 500 μA (see Table 2). Hence, we can postulate that during a standby period, the eventual self-discharge of the SC in the VRFC would have a negligible effect.

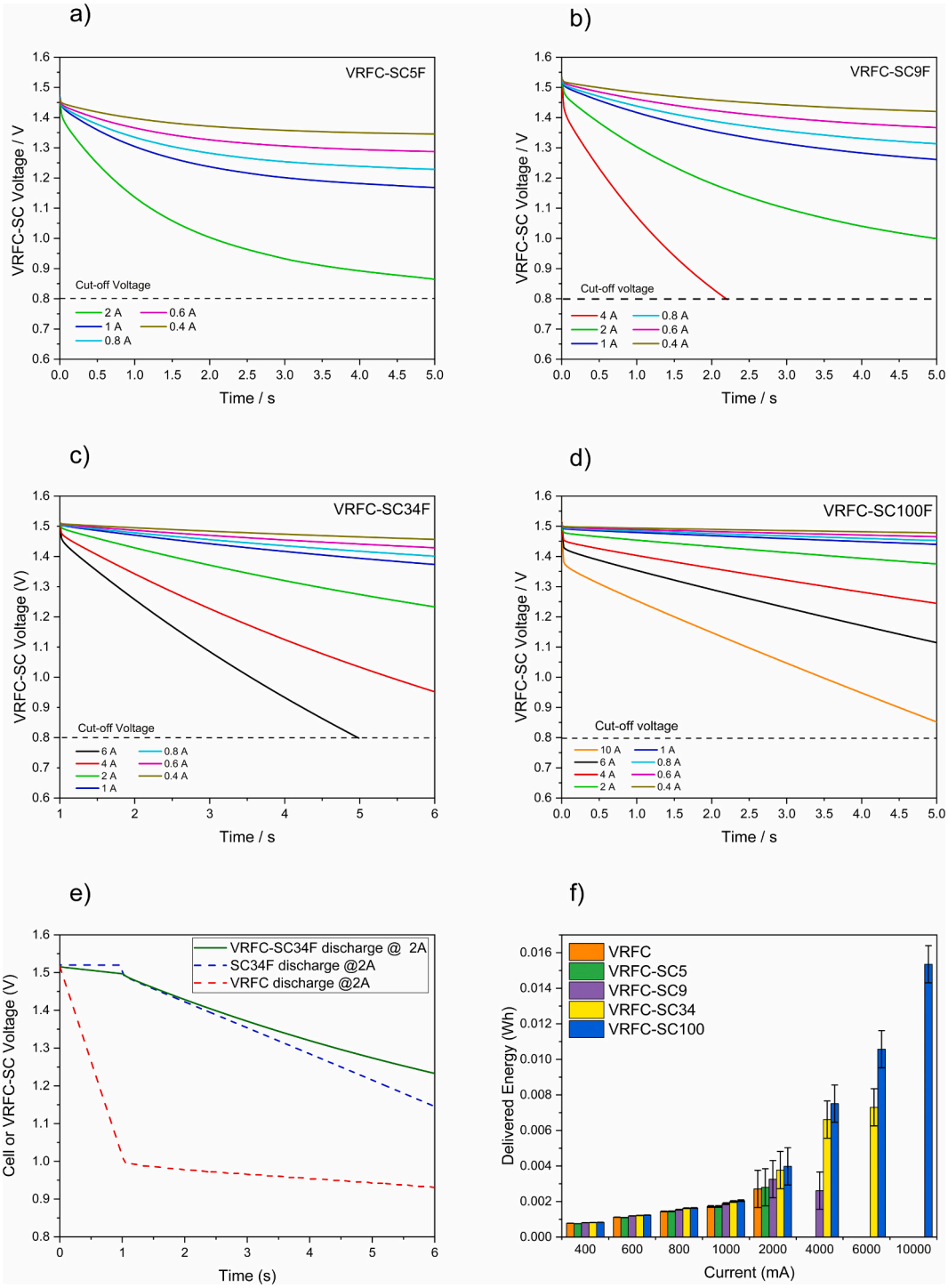

Fig. 3. a), b), c) and d) discharge profiles of the 4 different VRFC-SC systems during 5 s-pulse discharges at different discharging currents. e) Discharge profiles of the single VRFC, the single SC34F and of the hybrid system VRFC-SC34F during 5 s-galvanostatic pulses at 2 A. f) Energy delivered over 5 s-pulse discharges at different currents by the single VRFC cell and by the hybrid VRFC-SC systems featuring different commercial SCs. Experimental tests were conducted at RT. The starting SOC of the VRFC is 100%.

3.1.4. Modelling results and test comparison

This section explores the influence of supercapacitor properties on the performance of a hybrid VRFC-SC system. Section 3.1.4.1 analyses the effect of the supercapacitor's ESR on current distribution and discharge dynamics, while Section 3.1.4.2 investigates the impact of capacitance on energy delivery, highlighting the trade-off between performance and system sizing.

3.1.4.1. Effect of the supercapacitor equivalent series resistance on the system. We examine two distinct VRFC-SC systems composed of the same VRFC and two different SCs featuring the same 15F capacitance and different ESR of 0.02 Ω (SC1) or 0.11 Ω (SC2). The maximum voltage is the same and equal to 1.5 V corresponding to a VRFC SOC of 100%. These values are examples used to numerically assess the effect of the ESR on the system. All the input data implemented in the model for this analysis are reported in Table S13. Utilizing the Equations

mentioned in section 2.1.4, it is possible to plot the currents flowing in the branches of these two hybrid systems, as exemplified in Fig. 4a. Both systems maintain a constant current of 2 A through the external load. During discharge, while the overall generated current remains constant, the currents in the SC and VRFC branches vary over time. In the SC branch, the current decreases from its maximum value to nearly 0 A within 40 s. Conversely, in the VRFC branch, the current initially rises and stabilizes at approximately 2 A after 40 s, sustaining the entire current flowing through the external load. At the beginning of the discharge ($t = 0$ s), the current distribution in the two branches depends on the ESR of the SC branch (R_{SC}). With SC1, most of the total load current (2 A) flows through the SC branch initially, due to the lower internal resistance R_{SC}. Similarly, in the case of SC2, most of the current flows through its branch, although at a lower magnitude than 2 A, because of its higher R_{SC} compared to SC1 (0.11 Ω vs. 0.02 Ω). Despite the different R_{SC} values, the SC capacitance influences the transient duration similarly in both cases, as both SCs possess a capacitance of 15 F.

Fig. S5 compares the simulated and experimental discharge voltage profiles of VRFC-SC system during discharges at 1 A and 2 A, even longer than 5 s for at 100% SOC, and for a short pulse at 800 mA and 20% SOC. The simulation agrees well with the experimental profile, showing a maximum relative error below 3% and validating the simplified model for the VRFC-SC system.

3.1.4.2. Effect of the supercapacitor capacitance on the system. To investigate the impact of SC capacitance (SC size) on hybrid system energy performance (5 s-pulse discharge), we employed the model, utilizing values measured during the test conducted on the single devices and on the systems. Using the Equations listed in Section 2.1.4 it is possible to estimate the energy deliverable from the system varying the capacitance and discharging at the same current. The input values used in the model correspond to the VRFC and SCs specifications reported in Table 2 and Table S13 while v_L is set at 1.5 V. Fig. 4b depicts the delivered energy values obtained through the model (black points) and compares them with the delivered energy measured during the test of four tested systems, for a discharge current of 2 A. Fig. S7 reports the computed and experimental trends for discharge currents of 600 mA, 800 mA and 1 A.

It is noticeable that the model provides a good reliability in the evaluation of the pulsed energy. If we increase the value of the combined capacitance to a higher value, such as 300 F, the result given by the model is the one reported in Fig. 4b. It reveals that increasing capacitance enhances delivered energy up to an asymptotic value. This underscores that there is a limit to the deliverable energy by the system also using the highest capacitances. Rather, the SC capacitance should be tailored to achieve a deliverable energy corresponding to the knee of the curve, which can be extrapolated using different approaches. One possible method to identify the knee point consists in determining the point with the maximum distance from the straight line connecting the first and last points of the delivered energy–capacitance curve. According to this criterion, for the case shown in Fig. 4b, the knee point is located at approximately 75 F.

3.2. Life cycle assessment and sensitivity analysis

Fig. 5a displays the GWP of the *production* of a HESS with direct connection (A) compared to a HESS with converter-based (B) connection, while Fig. 5b presents the GWP of the *use phase*. In Fig. 5c, both phases were combined. Environmental impacts were determined for the base case and for the five cases of the sensitivity analysis (Sens. 1 – 5), respectively. Indicator values for all other environmental impact categories are provided in the SI. Fig. 5d provides a different depiction of the results of the sensitivity analysis, comparing the effects on all impact indicators investigated.

In the base case, the VRFB clearly caused the major impact on the GWP of the system's production phase (>94%). This was also true for most other impact indicators investigated, as displayed in the SI. The high environmental impacts of a VRFB's production phase are mainly caused by vanadium pentoxide (V_2O_5), which is used as active component in its electrolyte [35,36,45]. The GWP of HESS production increased with increasing SC size; however, the VRFB remained the single component with the largest impact. Despite increasing the SC power, the production of the SC continued to play a minor role regarding GWP for all cases investigated and irrespectively of the connection type. The higher GWP of HESS production at larger SC sizes can mainly be attributed to the larger AC-DC inverter and DC-DC converters.

In the base case, the GWP of HESS production with converter-based connection was 21% higher than with passive connection. However, the sensitivity analysis (Sens. 1 – 5) demonstrated that this relative difference increased with increasing SC size: assuming a SC power of 80 MW (Sens. 5), which would be eighty times the power of the VRFB, the HESS with passive connection exhibited a GWP of 0.095 kg CO_2-eq kWh^{-1}, while the HESS with converter-based connection showed a 27% higher GWP of 0.140 kg CO_2-eq kWh^{-1}.

Fig. 5b presents the GWP of the use phase. The energy losses during

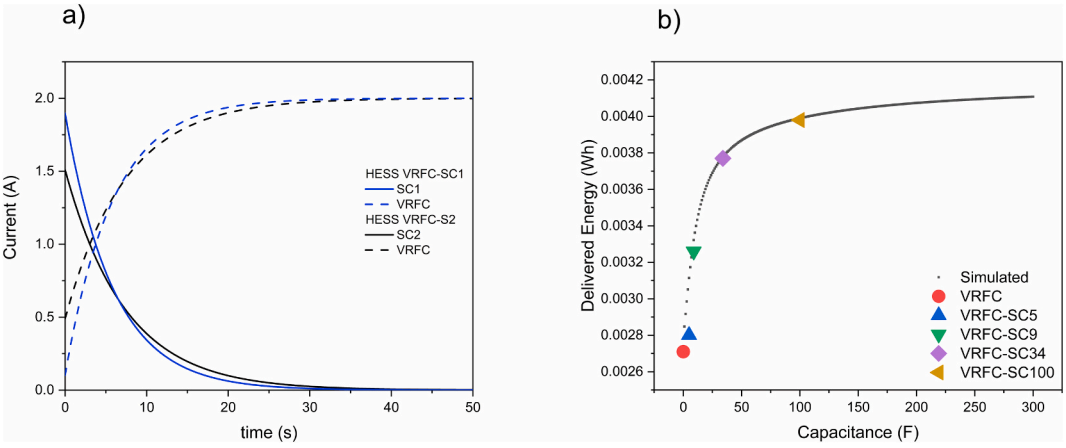

Fig. 4. a) currents flowing in the separate SC (solid line) and VRFC (dashed line) branches during discharge of two different VRFC_SC hybrid systems discharging at 2 A. the blue lines refer to the HESS with SC1, the black lines refer to the HESS with SC2, b) energy delivered by the VRFC-SC hybrid system over 5-s pulses at 2 A vs SC capacitance. The black dots are calculated using the model; coloured markers represent the results obtained during the parallel connection test between the VRFC and the commercial SCs. Experimental tests were conducted at RT . The starting SOC of the VRFC is 100%. (For interpretation of the references to colour in this figure legend, the reader is referred to the web version of this article.)

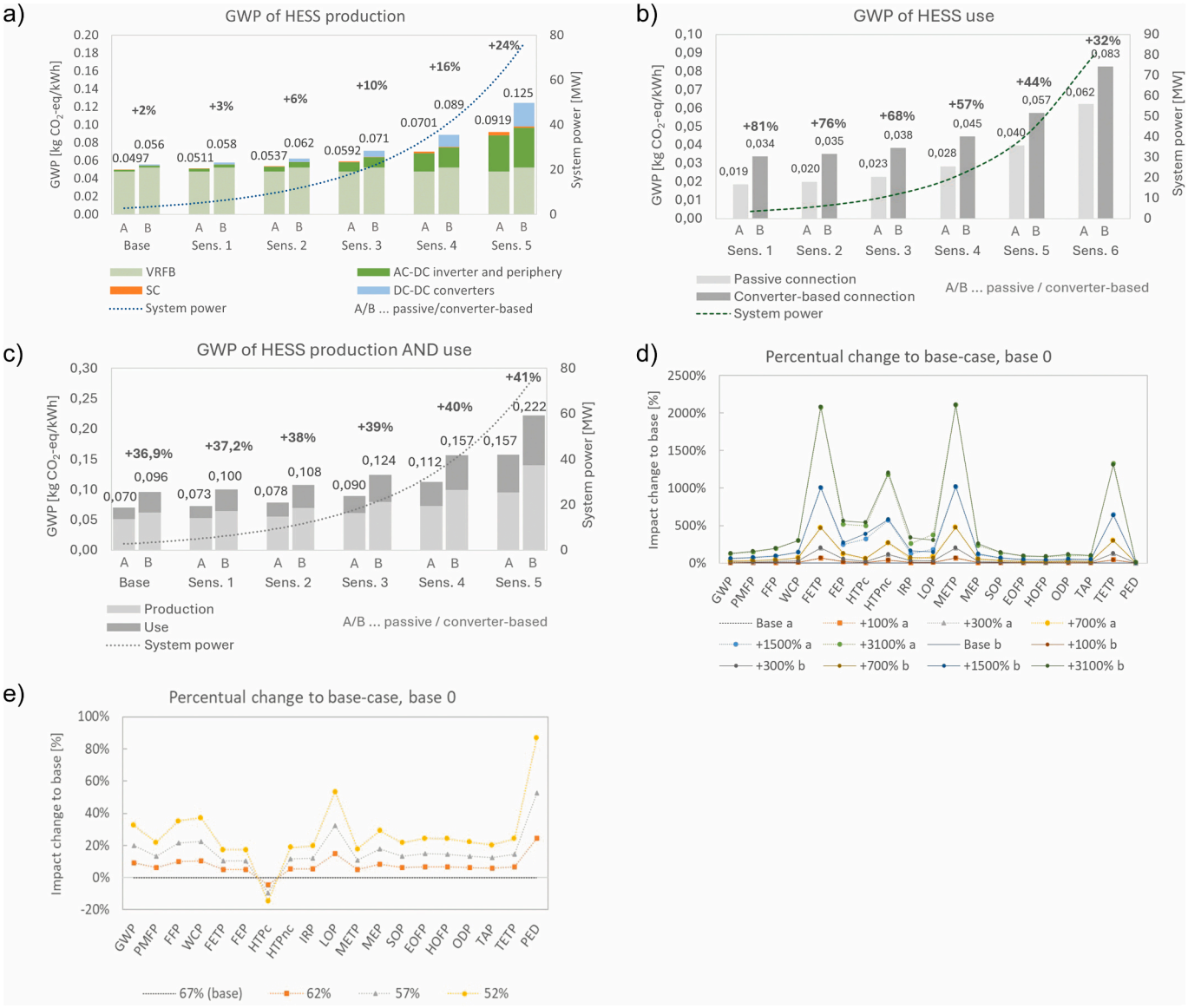

Fig. 5. a) global warming potential of hess production, b) global warming potential of hess use, and c) global warming potential of HESS production and use, for the base case and for sensitivity cases, respectively. d) results of sensitivity analysis of HESSs with passive (A) and converter-based (B) connection, altering HESS power (production and use, base = 2.5 MW SC). e) Results of sensitivity analysis of HESS with passive connection, altering round-trip efficiency from 67% to 62, 57 and 52% (production and use, basic configuration).

charging and discharging of the HESS caused the majority of the GWP in the base case and for Sens. 1 – 3. However, in Sens. 4 and 5, the impact of the AC-DC inverter exchange surpassed that of the energy losses. This applied for both connection types. In contrary to the production phase, the relative difference between the HESS with converter-based connection and passive connection decreased with increasing SC size. This can be attributed to the SC exchange, which showed a stronger increase with increasing SC size in case of the direct connection (triple number of SC cells) than for the converter-based connection. The GWP of the system's energy losses stayed constant with increasing SC size, and the GWP of the inverter exchange was the same for both connection types.

Comparing the results for the production and use phase (Fig. 5c) revealed that the production phase had a higher GWP than the use phase in all cases analysed, for both connection types. However, this only applies when charging the HESS with renewable power, as was modelled here. If applying a conventional electricity mix, the GWP of the use phase would be significantly higher. In the base case, the total GWP of HESS production and use amounted to 0.070 kg CO_2-eq kWh^{-1} for the passiveconnection and to 0.096 kg CO_2-eq kWh^{-1} for the converter-based connection. The difference between the HESS with passive connection and converter-based connection increased from 37% in the base case to 41% for Sens. 5. Detailed results for the sensitivity analysis of HESS production and use for all impact values are provided in Fig. 5d. A change of the SC power by + 3 100% to 80 MW led to a specifically high reaction of up to + 2 100% in FETP, HTPnc, METP and TETP. The effects on GWP were less pronounced and amounted to approximately + 125% for the passive connection and + 132% for the converter-based connection.

Fig. 5e presents the results of the second sensitivity analysis on the round-trip efficiency of the passive HESS. If the efficiency were drop from 67% to 52%, the GWP for production and use of the passively connected HESS would increase by 32% to 0.093 kg CO_2-eq kWh^{-1}. In this case, the GWP benefits of avoiding DC/DC converters would be nearly cancelled out by added electricity losses, leaving the passive HESS with a specific GWP close to that of the converter-based system.

The SC architecture assessed in this LCA uses an acetonitrile organic electrolyte. In contrast, aqueous electrolytes typically are not only cheaper and less hazardous but are also expected to reach the required system voltage in a HESS with passive connection. We assume that the acetonitrile electrolyte can be replaced on a 1:1 mass basis by a WiSE ammonium-acetate electrolyte (30 mol/kg). An LCA comparison showed that the latter exhibits far lower environmental impacts per kg across all indicators, with a GWP of only about 9% of acetonitrile (Fig. S5, SI). This suggests that the GWP contribution of the SC in a directly connected HESS could potentially be reduced further by applying an aqueous SC electrolyte. Still, the use of an aqueous electrolyte in the current SC design, the integration of this "green" SC in the passively connected HESS, and the assumptions described here, remain to be validated experimentally.

3.3. Economic assessment

The total project costs presented for the different HESS configurations represent the investment required for a turnkey facility and include both the costs of the main components and the associated additional and indirect costs. The main cost drivers are the VRFB, the SC, and PCS. For an active connection, the PCS comprises DC/DC converters for both the VRFB and the SC as well as an AC/DC inverter for grid connection, whereas for a passive connection only an AC/DC inverter is required. Additional and indirect costs cover expenditures for civil works, component assembly, process control and electrical engineering (materials and installation), site equipment, safety testing, quality control, engineering, construction and assembly supervision, commissioning, regulatory approvals, and contingencies. The resulting total project costs should be interpreted as indicative benchmarks rather than exact values, as actual costs depend strongly on project-specific conditions (e.g., building requirements or non-containerized implementations). Note that reported component costs in the literature or manufacturer data sheets typically exclude such additional and indirect costs and therefore underestimate the investment required for a fully operational system. Fig. 6 illustrates the calculated CAPEX and cost shares of the main components and additional and indirect costs for the "Base" and "S5" HESS configurations in 2022 and 2050, considering different connection types (active/passive) and SC electrolytes (organic/aqueous).

In 2022, additional and indirect costs account for approximately 46% of total project costs across all configurations, corresponding to a Lang factor of 1.85. By 2050, this share is projected to decrease slightly to approximately 39% (Lang factor 1.65), mainly due to reduced contingencies. These values are substantially lower than typical Lang factors of around 3 for conventional industrial facilities, reflecting the higher degree of prefabrication and reduced assembly complexity of containerized HESS components. The cost structure is primarily influenced by the connection type (active or passive), the system configuration (especially SC power), and the SC electrolyte (organic or aqueous), while temporal effects (until to 2050) play a minor role. In the "Base – active/organic" configuration, the SC contributes only approximately 3% in 2022 to 4% in 2050 of total project costs, the PCS 13 to 17%, and in contrast the VRFB about 38 to 39%. In the high-power "S5 – active/organic" configuration, the overall cost structure shifts. The SC share increases to 13 to 15% and the PCS to 35 to 40%, while the VRFB share decreases to approximately 6%. For passive configurations, the elimination of DC/DC converters halves PCS costs compared to active connections, but SC costs triple due to the requirement for three times the number of cells. Using an aqueous electrolyte reduces SC costs, making the "passive/aqueous" configuration the lowest-cost option among those analysed. Fig. 7 summarizes the total specific power- and energy-related project CAPEX for all configurations and includes scaling effects, with

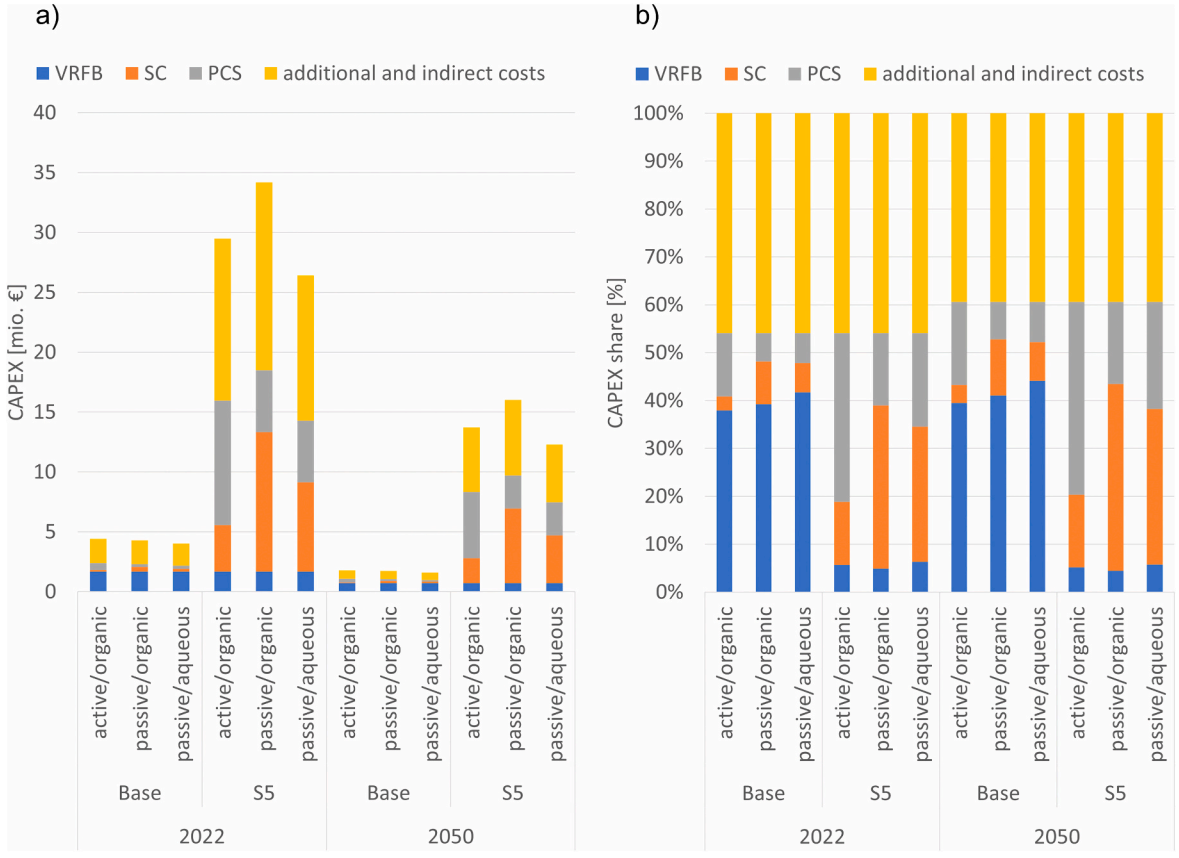

Fig. 6. a) Cost share and b) Cost share % of main components as well as additional and indirect costs for the HESS configurations "Base" and sensitivity "S5" in the years 2022 and 2050 for different connection types (active/passive) and SC types (organic/aqueous).

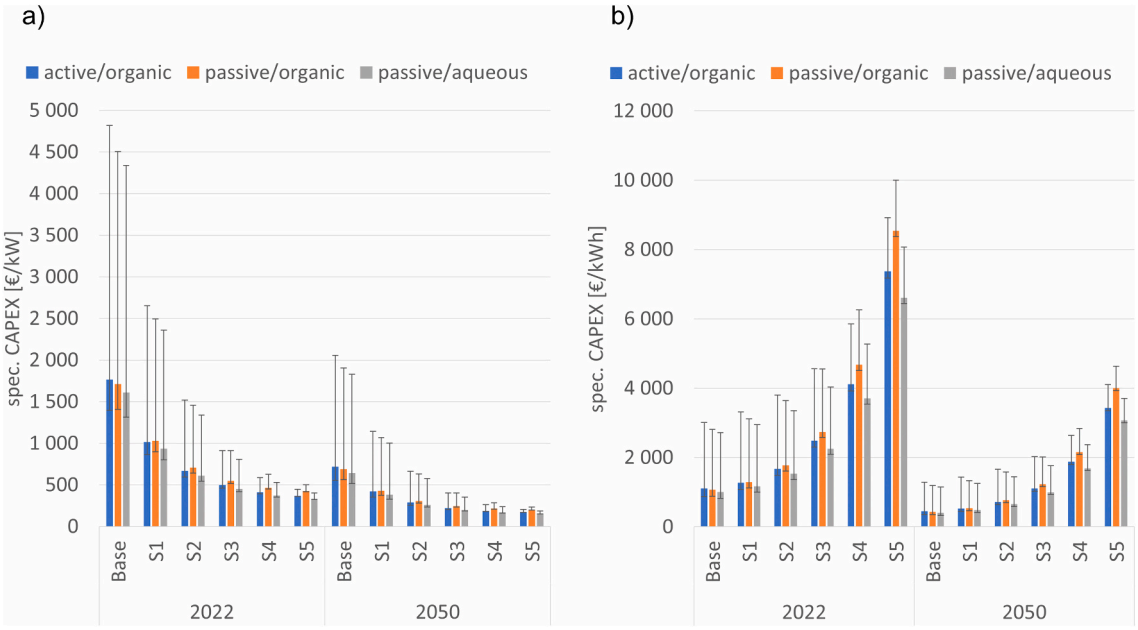

Fig. 7. Total spec. a) power and b) energy-related CAPEX of HESS. Bandwidth error indicator: lower value – reference system size times 10; upper value – reference system size times 0.10. [Base: SC 2.5 MW/VRFB 1 MW/4MWh; S1: SC 5 MW/VRFB 1 MW/4MWh; S2: SC 10 MW/VRFB 1 MW/4MWh, S3: SC 20 MW/VRFB 1 MW/4MWh, S4: SC 40 MW/VRFB 1 MW/4MWh, S5: SC 80 MW/VRFB 1 MW/4MWh].

system sizes varied by factors of 0.1 (indicated by the upper bandwidth error) and 10 (indicated by the lower bandwidth error).

Five key dependencies were identified: i) the prospective reduction in CAPEX due to technological learning (economies of scale by cumulative production volume), ii) the influence of up- and down-scaling (economies of unit scale), iii) the impact of the HESS configuration (variation in the rated power of the SC, iv) the effect of the connection type ("active" or "passive"), and v) the choice of electrolyte for the SC ("organic" or "aqueous"). Between 2022 and 2050, specific CAPEX decreases by about 60% across all configurations due to technological learning. Upscaling (by a factor of 10) reduces costs by roughly 20%, while downscaling (by a factor of 10) leads to a cost increase by a factor of 2.8. Increasing SC power strongly reduces power-related CAPEX but significantly increases energy-related CAPEX. Passive connections show slightly lower costs in the base configuration, whereas active connections become more cost-effective at higher SC power levels. Finally, aqueous SC electrolytes reduce specific costs by approximately 6 to 23% compared to organic electrolytes.

The results clearly indicate that the estimated HESS costs are sensitive to several key cost drivers. Additionally, there are uncertainties related to vanadium price volatility, future cost developments of supercapacitors (especially for emerging aqueous electrolyte concepts), converter efficiency improvements, and installation costs can significantly influence total project CAPEX. Further, although passive connection concepts reduce PCS and are therefore commonly associated with lower maintenance requirements, the increased number of SC cells may partially offset this advantage due to a potentially higher probability of cell failures and replacement needs. A comprehensive assessment of operation and maintenance costs, including component reliability and lifetime effects, is therefore identified as an important topic for future research. Consequently, the presented cost estimates should be interpreted as indicative benchmarks rather than precise forecasts, highlighting the importance of project-specific assessments and updated cost data when applying the proposed framework to real-world deployments. Overall, specific CAPEX of the HESS shows strong learning and scaling effects. While the connection type has a moderate influence, SC power and electrolyte choice are decisive cost drivers. Among the analysed configurations, the passive connection with an aqueous SC, results in the lowest costs, although an active connection combined with an aqueous SC may offer further cost reduction potential.

4. Conclusions

This study demonstrates the potential of directly integrating Vanadium Redox Flow Batteries with Supercapacitors to form a Hybrid Energy Storage system. The combination exploits the complementary features of these technologies, with the energy density of VRFBs synergistically paired with the high power density and rapid charge/discharge capabilities of SCs. Through experimental tests and modelling, we showed that the direct parallel connection of VRFB and SC at the cell level significantly enhances the system's ability to deliver energy during high-power pulses, while reducing the reliance on high-voltage SCs with organic electrolytes. Indeed, the absence of the power converter requires the two HESS branches to feature the same maximum voltages. A full-charged VRFC has an open circuit voltage (OCV) of about 1.5 V; commercial EDLCs, employing conventional organic electrolyte, can reach 3 V maximum voltage. Hence, this EDLC, if directly connected to a VRFC, works in a cell voltage range that is limited by the VRFC OCV. Given that the energy and power performance of the EDLC depends on its cell voltage, reaching half of its cell voltage also means that the EDLC cannot exploit all of its energy and power maximum performance. In turn, this has an impact on the overall system costs. The lower cell voltage opens the possibility of using EDLCs that operate with alternative, more environmentally friendly electrolytes, like aqueous solutions. They are interesting candidates for designing a HESS where the VRFC and SC are directly connected, because they feature maximum voltages that might be compatible with VRFC OCV. Of course, the inherent value of using an aqueous electrolyte is to provide a big improvement in terms of sustainability of the SC and the HESS itself: avoiding the conventional organic electrolytes of SC means avoiding safety issues, such as flammability, toxicity, and teratogenicity. However, water-based supercapacitors, like those employing water-in-salt electrolytes, are still in the development stage and currently exhibit a technology readiness level $<$ 4, as they are available only at laboratory scale. Moreover, our modelling approach provided a practical methodology to size SCs optimally in hybrid configurations, avoiding oversizing and reducing costs. The

results highlight the importance of tailoring the SC characteristics to maximize energy delivery while reducing unnecessary economic and environmental impacts.

Indeed, a life cycle assessment and an economic analysis were carried out to evaluate the potential benefits of a passive VRFB-SC connection. The LCA showed that the relative advantages regarding GWP of a HESS with direct connection to a system with converter-based connection increase with increasing system power. There only exist very few LCA studies on SCs in literature [32 46–48], and those available are based on small cells (2.7 V, 0.005 Wh) that were upscaled. Hence, an LCA of a real SC module in the MW scale based on manufacturer data would be of high interest, to verify the approximations made by means of the small cells. However, the relative impact of the SC on the GWP of the HESS is minor, even at high SC power. By contrast, the impact of the DC-DC converters, in case of the converter-based connection, and of the AC-DC inverter on the system's GWP is strongly increasing with increasing SC power. Therefore, data verification based on real large-scale units, or an approximation of scaling effects would be interesting for future research.

From an economical point of view the HESS cost depends on connection type (active or passive), system configuration and SC size and type (organic or aqueous). The configuration that achieves the lower project costs is the one featuring a passive connection with aqueous SCs. Overall, the integration of experimental and simulation data with an assessment of economic and environmental impacts confirms the feasibility and potential competitiveness of the VRFB-SC hybrid system. This evaluation underscores the system's relevance as a sustainable and efficient solution for energy storage, particularly for applications requiring short-term high-power outputs combined with long-term energy storage capacity.

5. Limitations of the study and future developments

One of the limitations of the present study is related to the inherent constraints of laboratory-scale testing. We evaluated only four configurations of the VRFC–SC system, and to enable a more comprehensive assessment, further configurations should be investigated. The benefit of the SC coupling at high currents must be investigated in an upscaled system. Indeed, the obtained results could vary depending on the design and operating parameters, which must be considered during the system design for realistic operating conditions The research should also explore alternative scenarios, such as comparisons with different connection types, supercapacitor models, system stability assessments, extended discharge experiments, and the influence of varying VRFC cell SOC on dynamic performance outcomes. Further research is in progress to investigate the long-term operation and cycle life of the VRFC, SC, and the integrated passive VRFC–SC system, and to assess their capacity to operate under high current conditions without adjusting the pump rate. Extended cycling tests and accelerated aging studies must be conducted to evaluate long-term performance and reliability. The AC/DC converter regulates the DC bus voltage; however, solutions, such as passive circuits, require evaluation to manage internal balancing currents and reduce the risk of overvoltage during the charging phase, which is outside the scope of the present work.

Moreover, the transition from laboratory-scale systems (4 cm^2) to industrial applications may involve considerable engineering challenges. However, the VRFC provider (Pinflow) has already demonstrated strong transferability between results obtained from a 20 cm^2 single cell and a 608 cm^2 20-cell pilot stack [49].

In addition, in an ideal upscaled system, each supercapacitor should be paired with a single cell in order to minimise the need for balancing circuits. However, from a practical perspective, this configuration presents several challenges. A more detailed evaluation of practical implementation—including system integration and maintenance procedures—is necessary to support real-world application. Furthermore, as outlined in the introduction, the modelling approach remains relatively simple. Although this provides rapid responses, it also introduces a margin of error. Both the experimental and modelling components require deeper analysis, which will likely contribute to the development of a more realistic VRFC-SC system. At this stage, as indicated in the introduction, the research serves as an exploratory effort to understand the operational behaviour of the VRFC system and the modelling process.

From an economic assessment point of view: while this study focused on the assessment of various HESS configurations and connection types with an emphasis on capital expenditure, a comprehensive evaluation of economic performance indicators such as LCOE, NPV, and payback periods remains subject to future research, as such an analysis would require application-specific operational profiles and market assumptions that go beyond the scope of this work. Future work should also address the detailed engineering challenges associated with scaling, integration, and operation of HESS in real-world applications, which go beyond the economic focus of this study. Determining the round-trip efficiency of the HESS in real use cases would be highly relevant for the LCA, as electricity losses account for a significant share of the system's overall GWP. Moreover, the operability of the system with aqueous SC electrolytes needs to be tested, which is a prerequisite for assessing their actual environmental benefits.

CRediT authorship contribution statement

Monica Giovannucci: Conceptualization, Formal analysis, Investigation, Methodology, Software, Validation, Visualization, Writing – original draft, Writing – review & editing. **Elisabetta Petri:** Investigation, Writing – original draft, Writing – review & editing. **Alessandro Brilloni:** Conceptualization, Investigation, Visualization. **Eva-Maria Heigl:** Conceptualization, Investigation, Visualization, Writing – original draft, Writing – review & editing. **Andreas Zauner:** Conceptualization, Investigation, Visualization, Writing – original draft, Writing – review & editing. **Estanis Oyarbide:** Conceptualization, Writing – review & editing. **Jiří Charvát:** Investigation, Validation. **Francesca Soavi:** Conceptualization, Project administration, Resources, Writing – original draft, Writing – review & editing.

Declaration of competing interest

The authors declare the following financial interests/personal relationships which may be considered as potential competing interests: [Francesca Soavi reports financial support was provided by European Commission. Francesca Soavi reports financial support was provided by Italian Minister for Ecological Transition, MiTE. If there are other authors, they declare that they have no known competing financial interests or personal relationships that could have appeared to influence the work reported in this paper.].

Acknowledgement

This project has received funding from the European Union's Horizon 2020 research and innovation programme under grant agreement No. 96355 (HyFlow).

This work was also supported by the MIAMI Project 2022-2025 – Italian Minister for Ecological Transition, MiTE codice proposta CSEAA_000114. F.S. also acknowledges University of Bologna funding under the program Ricerca Fondamentale Orienata (RFO).

Appendix A. Supplementary data

Supplementary data to this article can be found online at https://doi.org/10.1016/j.ecmx.2026.101785.

Data availability

Data will be made available on request.

References

[1] Ye R, Henkensmeier D, Yoon SJ, Huang Z, Kim DK, Chang Z, et al. Redox flow batteries for energy storage: a technology review. J Electrochem Energy Convers Storage 2018;15(1):010801. https://doi.org/10.1115/1.4037248.

[2] Jiang Y, Liu Z, Ren Y, Tang A, Dai L, Wang L, et al. Maneuverable B-site cation in perovskite tuning anode reaction kinetics in vanadium redox flow batteries. J Mater Sci Technol 2024;186:199–206. https://doi.org/10.1016/j.jmst.2023.12.005.

[3] Fan H, Liu K, Zhang X, Di Y, Liu P, Li J, Hu B, Li H, Ravivarma M, Song J. Spatial structure regulation towards armor-clad five-membered pyrroline nitroxides catholyte for long-life aqueous organic redox flow batteries, eScience, 4 (2024) 100202. Doi: 10.1016/j.esci.2023.100202.

[4] Sánchez-Díez E, Ventosa E, Guarnieri M, Trovò A, Flox C, Marcilla R, et al. Redox flow batteries: Status and perspective towards sustainable stationary energy storage. J Power Sources 2021;481:228804. https://doi.org/10.1016/j.jpowsour.2020.228804.

[5] Lourenssen K, Williams J, Ahmadpour F, Clemmer R, Tasnim S. Vanadium redox flow batteries: a comprehensive review. J Storage Mater 2019;25:100844. https://doi.org/10.1016/j.est.2019.100844.

[6] Schubert C, Hassen WF, Poisl B, Seitz S, Schubert J, Oyarbide Usabiaga E, Gaudo PM, Pettinger KH, Hybrid energy storage systems based on redox-flow batteries: recent developments, challenges, and future perspectives, *Batteries*, 9(4), (2023), 211, Doi: 10.3390/batteries9040211.

[7] Pettinger KH, Project HyFlow: Development of a sustainable hybrid storage system based on high power vanadium redox flow battery and supercapacitor—technology; funded by the European Union's Horizon 2020 research and innovation programm under grand agreement No 963550; European Commission: Brussels, Belgium, (2020),.

[8] Schütter C, Pohlmann S, Balducci A. Industrial requirements of materials for electrical double layer capacitors: impact on current and future applications. Adv Energy Mater 2019;9:1900334. https://doi.org/10.1002/aenm.201900334.

[9] Béguin F, Presser V, Balducci A, Frackowiak E. Carbons and electrolytes for advanced supercapacitors. Adv Mater 2014;26:2219–51. https://doi.org/10.1002/adma.201304137.

[10] Lannelongue P, Bouchal R, Mourad E, Bodin C, Olarte M, Le Vot S, et al. "Water-in-Salt" for supercapacitors: a compromise between voltage, power density, energy density and stability. J Electrochem Soc 2018;165(3):A657–63. https://doi.org/10.1149/2.0951803jes.

[11] Amiri M, Bélanger D. Physicochemical and electrochemical properties of water-in-salt electrolytes. ChemSusChem: Chem Sustain Energy Mater 2021;14:2487–500. https://doi.org/10.1002/cssc.202100550.

[12] El Halimi MS, Poli F, Mancuso N, Olivieri A, Mattioli EJ, Calvaresi M, et al. Circumneutral concentrated ammonium acetate solution as water-in-salt electrolyte. Electrochim Acta 2021;389:138653. https://doi.org/10.1016/j.electacta.2021.138653.

[13] Gorji SA, Sahebi HG, Ektesabi M, Rad AB. Topologies and control schemes of bidirectional DC–DC power converters: an overview. IEEE Access 2019;7:117997–8019. https://doi.org/10.1109/ACCESS.2019.2937239.

[14] Etxeberria A, Vechiu I, Camblong H, Vinassa JM, Hybrid energy storage systems for renewable energy sources integration in microgrids: a review, 2010 Conference Proceedings IPEC, Singapore: IEEE, (2010), 532–537, Doi: 10.1109/IPECON.2010.5697053.

[15] Babu TS, Vasudevan KR, Ramachandaramurthy VK, Sani SB, Chemud S, Lajim RM. A comprehensive review of hybrid energy storage systems: converter topologies, control strategies and future prospects. IEEE Access 2020;8:148702–21. https://doi.org/10.1109/ACCESS.2020.3015919.

[16] Zheng JP, Jow TR, Ding MS. Hybrid power sources for pulsed current applications. IEEE Trans Aerosp Electron Syst 2001;37:288–92. https://doi.org/10.1109/7.913688.

[17] Martellucci L, Dell'Aria M, Capata R. Experimental Analysis and simulation of mixed Storage with Lithium-Ion Batteries and Supercapacitors for a PHEV. Energies 2023;16:3882. https://doi.org/10.3390/en16093882.

[18] Palma L, Enjeti P, Howze JW, An approach to improve battery run-time in mobile applications with supercapacitors, IEEE 34th Annual Conference on Power Electronics Specialist, 2003. PESC '03, Acapulco, Mexico, 2, (2003), 918-923, Doi: 10.1109/PESC.2003.1218178.

[19] J⌀rgensen KL, Mira MC, Zhang Z, Andersen MAE, Review of high efficiency bidirectional dc-dc topologies with high voltage gain, in: 2017 52nd International Universities Power Engineering Conference (UPEC), Heraklion, Greece, (2017), 1-6 https://doi.org/10.1109/UPEC.2017.8231916.

[20] Li W, Joós G, A power electronic interface for a battery supercapacitor hybrid energy storage system for wind applications, 2008 IEEE Power Electronics Specialists Conference, Rhodes, Greece, (2008), 1762-1768, Doi: 10.1109/PESC.2008.4592198.

[21] Jia H, Fu Y, Zhang Y, He W, Design of Hybrid Energy Storage Control System for Wind Farms Based on Flow Battery and Electric Double-Layer Capacitor, 2010 Asia-Pacific Power and Energy Engineering Conference, Chengdu, China, (2010),1-6, Doi: 10.1109/APPEEC.2010.5448720.

[22] Regulation (EU) 2023/1542 of the European Parliament and of the Council of 12 July 2023 concerning batteries and waste batteries, amending Directive 2008/98/EC and Regulation (EU) 2019/1020 and repealing Directive 2006/66/EC: Batteries Regulation, 2023. Accessed: Jul. 4 2024. [Online]. Available: https://eur-lex.europa.eu/eli/reg/2023/1542/ojoj.

[23] Zhou W, Zheng Y, Pan Z, Lu Q. Review on the battery model and SOC estimation method. Processes 2021;9(9):1685. https://doi.org/10.3390/pr9091685.

[24] Zhang L, Hu X, Wang Z, Sun F, Dorrell DG. A review of supercapacitor modeling, estimation, and applications: a control/management perspective. Renew Sustain Energy Rev 2018;81:1868–78. https://doi.org/10.1016/j.rser.2017.05.283.

[25] International Organization for Standardization, ISO 14040:2006(en), Environmental management - Life cycle assessment - Principles and framework, (2006), https://www.iso.org/obp/ui/.

[26] International Organization for Standardization, ISO 14044:2006(en), Environmental management - Life cycle assessment - Requirements and guidelines, (2006). https://www.iso.org/obp/ui/.

[27] Frischknecht R, Lehrbuch der Ökobilanzierung, Springer Spektrum Berlin, Heidelberg, (2020), https://doi.org/10.1007/978-3-662-54763-2.

[28] Guinée JB, Gorrée M, Heijungs R, Huppes G, Kleijn R, de Koning A, van Oers L, Wegener Sleeswijk A, Suh S, Udo de Haes HA, de Bruijn H, van Duin R, Huijbregts M, Handbook on Life Cycle Assessment. Operational Guide to the ISO Standards, 1st ed., Springer Dordrecht, (2002), Doi: 10.1007/0-306-48055-7.

[29] Curran MA, (ed.), Life Cycle Assessment Handbook. A Guide for Environmentally Sustainable Products, Wiley, (2012), Doi: 10.1002/9781118528372.

[30] Klöpffer W, Grahl B, Life Cycle Assessment (LCA): A Guide to Best Practice, Wiley-VCH, (2014), 1-396, Doi: 10.1002/9783527655625.

[31] Heigl E-M, Schäffer M, Zeilerbauer L, Zauner A, Lindorfer J, Ott J, et al. Life cycle assessment of a novel hybrid energy storage system: environmental hotspots and sustainability options based on experimental insights. J Storage Mater 2025;132 (Part B):117705. https://doi.org/10.1016/j.est.2025.117705.

[32] Jiao Y, Månsson D. Greenhouse gas emissions from hybrid energy storage systems in future 100% renewable power systems – a swedish case based on consequential life cycle assessment. J Storage Mater 2023;57:106167. https://doi.org/10.1016/j.est.2022.106167.

[33] Sphera, LCA for Experts 10.7 software and professional database, https://sphera.com/software-fuer-die-lebenszyklus-beurteilung-lca/?lang=de.

[34] Ecoinvent Association, ecoinvent database: sustainability assessment, https://ecoinvent.org/database/.

[35] Blume N, Becker M, Turek T, Minke C. Life cycle assessment of an industrial-scale vanadium flow battery. J Ind Ecol 2022;26:1796–808. https://doi.org/10.1111/jiec.13328.

[36] Weber S, Peters JF, Baumann M, Weil M. Life cycle assessment of a vanadium redox flow battery. Environ Sci Technol 2018;52:10864–73. https://doi.org/10.1021/acs.est.8b02073.

[37] Huijbregts MAJ, Steinmann ZJN, Elshout PMF, Stam G. ReCiPe2016: a harmonised life cycle impact assessment method at midpoint and endpoint level. Int J Life Cycle Assess 2017;22:138–47. https://doi.org/10.1007/s11367-016-1246-y.

[38] VDI, VDI 4600 Kumulierter Energieaufwand - Begriffe, Definitionen, Berechnungsmethoden, VDI, https://www.vdi.de/.

[39] Kupfer T, GaBi Databases & Modelling Principles, (2021) [Online], www.sphera.com.

[40] Perry RH, Green DW, Maloney JO, editors. Perry's Chemical Engineers' Handbook. 7th ed. New York: McGraw-Hill; 1997.

[41] Peters MS, Timmerhaus KD, Plant Design and Economics for Chemical Engineers, 4th ed., McGraw-Hill Chemical Engineering Series, McGraw-Hill, New York, (1991).

[42] Turton R, (Ed.), Analysis, Synthesis, and Design of Chemical Processes, 5th edition, Prentice Hall International Series in the Physical and Chemical Engineering Sciences, Prentice Hall, Boston, (2018).

[43] Weber KH. Engineering verfahrenstechnischer Anlagen: Praxishandbuch mit Checklisten und Beispielen. Heidelberg: Auflage SpringerVieweg; 2016. p. 2.

[44] Zauner et al., Deliverable D3.6 – Market potential analysis, HyFlow, (2024), https://cordis.europa.eu/project/id/963550/results.

[45] da Silva Lima L, Quartier M, Buchmayr A, Sanjuan-Delmás D, Laget H, Corbisier D, Mertens J, Dewulf J. Life cycle assessment of lithium-ion batteries and vanadium redox flow batteries-based renewable energy storage systems. Sustainable Energy Technol Assess 2021;46. https://doi.org/10.1016/j.seta.2021.101286.

[46] Cossutta M, Vretenar V, Centeno TA, Kotrusz P, McKechnie J, Pickering SJ. A comparative life cycle assessment of graphene and activated carbon in a supercapacitor application. J Clean Prod 2020;242:118468. https://doi.org/10.1016/j.jclepro.2019.118468.

[47] Kamal Kamali A, Glogic E, Keppetipola NM, Sonnemann G, Toupance T, Cojocaru L, Prospective Life Cycle Assessment of Two Supercapacitor Architectures ACS Sustainable Chemistry & Engineering, 11 (44), (2023), 15898-15909, Doi: 10.1021/acssuschemeng.3c04007.

[48] Li Y, Han X, Nie L, Deng Y, Yan J, Roumpedakis TC, et al. Life cycle environmental hotspots analysis of typical electrochemical, mechanical and electrical energy storage technologies for different application scenarios: case study in China. J Clean Prod 2024;466:142862. https://doi.org/10.1016/j.jclepro.2024.142862.

[49] Charvát J, Pocedič J, Vrána J, Detailed investigation of VFB stack with a focus on single cell, The International Flow Battery Forum, Glasgow, UK, June 25–27, 2024.